PCCP

Physical Chemistry Chemical Physics

rsc.li/pccp
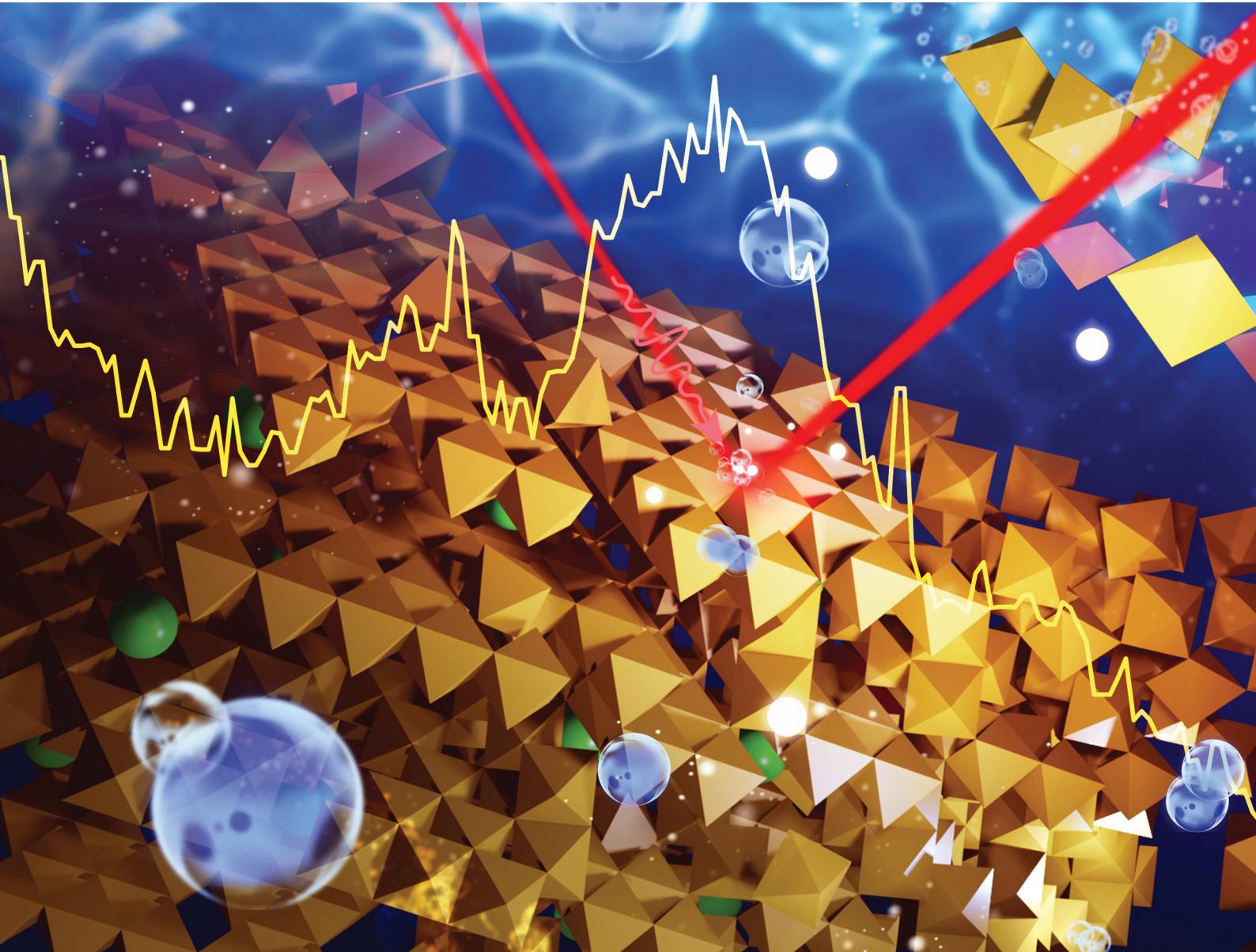
ROYAL SOCIETY
OF **CHEMISTRY**

REVIEW ARTICLE
Andreas Erbe, Marc Frederic Tesch, Martin Rabe *et al.*
Operando studies of Mn oxide based electrocatalysts
for the oxygen evolution reaction

PCCP
Owner Societies

REVIEW

Check for updates

Operando studies of Mn oxide based electrocatalysts for the oxygen evolution reaction

Andreas Erbe,*[a] Marc Frederic Tesch, [ID] *[b] Olaf Rüdiger, [ID] [b] Bernhard Kaiser,[c] Serena DeBeer [ID] [b] and Martin Rabe [ID] *[d]

Inspired by photosystem II (PS II), Mn oxide based electrocatalysts have been repeatedly investigated as catalysts for the electrochemical oxygen evolution reaction (OER), the anodic reaction in water electrolysis. However, a comparison of the conditions in biological OER catalysed by the water splitting complex $CaMn_4O_x$ with the requirements for an electrocatalyst for industrially relevant applications reveals fundamental differences. Thus, a systematic development of artificial Mn-based OER catalysts requires both a fundamental understanding of the catalytic mechanisms as well as an evaluation of the practicality of the system for industrial scale applications. Experimentally, both aspects can be approached using *in situ* and *operando* methods including spectroscopy. This paper highlights some of the major challenges common to different *operando* investigation methods and recent insights gained with them. To this end, vibrational spectroscopy, especially Raman spectroscopy, absorption techniques in the bandgap region and *operando* X-ray spectroelectrochemistry (SEC), both in the hard and soft X-ray regime are particularly focused on here. Technical challenges specific to each method are discussed first, followed by challenges that are specific to Mn oxide based systems. Finally, recent *in situ* and *operando* studies are reviewed. This analysis shows that despite the technical and Mn specific challenges, three specific key features are common to most of the studied systems with significant OER activity: structural disorder, Mn oxidation states between III and IV, and the appearance of layered birnessite phases in the active regime.

1. Introduction

The electrochemical oxygen evolution reaction (OER),

$$2H_2O \rightarrow O_2 + 4H^+ + 4e^- \qquad (1)$$

or

$$4OH^- \rightarrow O_2 + 2H_2O + 4e^-, \qquad (2)$$
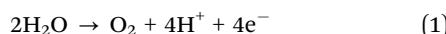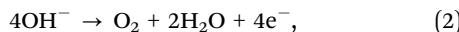
is the anodic partial reaction of electrochemical water splitting. The cathodic partial reaction of water splitting, the hydrogen evolution reaction (HER), can be employed for the production of "green" hydrogen, when renewable electricity sources are used.[1] However the OER half-cell reaction is generally considered the bottleneck of the water splitting reaction because the involved transfer of 4 electrons is kinetically challenging.[2]

Currently, the most effective anode materials for water splitting rely on expensive noble metals such as Ru or Ir. Thus, lowering the OER overpotential by catalysts based on earth-abundant materials and support materials is a significant goal on the way towards more economical hydrogen based energy storage systems and a decarbonized economy.

Biological oxygen evolution occurring in photosystem (PS) II is catalysed in an active center containing a $CaMn_4O_x$ cluster as the oxygen evolving complex (OEC).[3–5] Computational and spectroscopic investigations have contributed significantly to the understanding of the reaction mechanisms leading to the production of O_2 during photosynthesis.[6–10] Researchers have been tempted to ask whether simple synthetic Mn-based systems can take over the function of the PS II active complex in an electrochemical system, leading to a lot of interest in Mn-based OER electrocatalysts. These could act as alternatives to highly performing, but also rare and expensive systems based, *e.g.*, on Ir or Ru.[11]

For biological oxygen evolution, manganese was considered the "natural" choice for a catalyst, due to the combination of several properties such as its availability as soluble Mn^{II}, its versatile redox chemistry with reachable oxidation states and its aqueous coordination chemistry.[5] For industrial

[a] *Department of Materials Science and Engineering, NTNU, Norwegian University of Science and Technology, 7491 Trondheim, Norway*

[b] *Max Planck Institute for Chemical Energy Conversion, Stiftstr. 34-36, 45470 Mülheim an der Ruhr, Germany. E-mail: marc.tesch@cec.mpg.de*

[c] *Surface Science Laboratory, Department of Materials- and Earth Sciences, Technical University Darmstadt, Otto-Berndt-Str. 3, 64287 Darmstadt, Germany*

[d] *Max-Planck-Institut für Eisenforschung GmbH, Max-Planck-Str. 1, 40237 Düsseldorf, Germany. E-mail: m.rabe@mpie.de*

applications, its high abundance on Earth makes it attractive, as Mn is available at a low price and with relatively low criticality.[12–14] However, a fundamental difference between the requirements for OER catalysts in a biological system and in scenarios for the large-scale production of green hydrogen are the vastly varying current requirements. Biological O_2 production in the respiratory chain involves several transport steps. Thus, transport limitation will at some point limit the currents. At these rather low currents, a catalytic cycle has evolved that is made possible only by the high electronic and structural control of PSII as a supramolecular system.[6,15] Several technological approaches based on water splitting have been or are currently being developed, with very different requirements for the working conditions in which the required OER catalysts must persist.[16–19] For instance, moderate currents in the range of 10–20 mA cm^{-2} would be appropriate for solar water splitting applications, which however in most cases disallow extreme pH values and require specific optical or morphological properties.[17,20] On the other side, industrial zero gap alkaline water electrolyzers can operate at currents up to 1 A cm^{-2}, in a 20–30 wt% KOH electrolyte and at temperatures of up to 100 °C,[18,19] which differ significantly from the conditions in biological OERs. Yet, any economically useful catalyst should provide lifetimes in the range of years. Other aspects that require consideration for industrial applications are the costs and scalability of the catalyst preparation and electrode fabrication as well as robustness with respect to varying electrolyte compositions. Nevertheless, the high demand for affordable green energy storage technologies has triggered new research efforts towards Mn-based OER electrocatalysts.[11]

The mechanism of the dioxygen formation *via* heterogenous catalysis has been studied for decades (for a review see ref. 2). General schemes for metal oxide catalysts start from adsorbed OH at active surface (metal) sites, followed by single electron charge transfer steps to form M–O (terminal-oxo) species. The O–O bond formation may occur from adjacent M–O or M–OH sites or from a single site *via* peroxo intermediates.[2] However, the nature of the intermediates and the intermediate steps remain controversial and likely depend on the exact conditions and the catalyst. Beside such atomic understanding, a knowledge driven catalyst development requires a detailed understanding of the processes occurring at application-relevant electrodes including the support and an evaluation of the practicality of the system in applications. Experimentally, these insights are obtained by characterisation of the catalyst using '*in situ*' (*i.e.* in electrolyte "at the location" of the electrochemical process) and "*operando*" (*i.e.* "during the [electrochemical] process" itself) experiments.

The goal of electrochemical *in situ* and *operando* studies is the understanding of the chemical transformations taking place on the electrode surface (substrate and catalyst) as a function of potential or current. In spectroelectrochemical *in situ* experiments, the spectroscopic signature of a system is directly measured in a controlled environment, *e.g.*, at an electrode in the electrolyte under potential control. *Operando* spectroelectrochemistry is a sub-type of the *in situ* experiment,

which – for electrocatalytic applications – requires that a catalytic activity/selectivity is measured simultaneously to the spectroscopy.[21,22] In OER electrocatalysis, the current density provided by the potentiostat is often used to monitor the catalytic activity. This article will discuss the potential of such *operando* studies to foster the understanding of Mn catalysed OERs. To that end, first, general and Mn specific challenges for such *operando* spectroelectrochemical methods are discussed, followed by a short review of selected recent *in situ* and *operando* studies.

2. Mn oxide-based systems pose special analytical challenges

2.1 General challenges for *operando* methods

Challenge 1: *Operando* data do not necessarily yield unique information on the reaction mechanism. In general all *operando* studies represent an "inverse" problem of an especially challenging nature. Predicting the answer given by an experiment is straightforward when the underlying mechanism or system is known. The opposite process, *i.e.* determining the unknown mechanism from the experimental result, is tedious and often does not yield unambiguous solutions.

Challenge 2: The necessity for reference data. Many spectroscopic or scattering techniques rely on an analysis that is based and established in *ex situ* measurements, such as a knowledge-base obtained *e.g.* on pure, well defined compounds. The potentially unstable species that occur as intermediates during chemical reactions are not necessarily covered by such reference data and might therefore yield signals which are hard to understand by bare comparison to intrinsically stable reference compounds.

Computational models can help to overcome the lack of reference data and also help to solve the inverse problem. However, for electrocatalytic systems, approaches to correctly describe the electrode potentials in computations with a relevant system size in interfacial systems are just emerging.[23,24] The fact that Mn-based systems likely require an appropriate description of the correct spin state make calculations computationally expensive. Thus, such systems are not necessarily the best early adoption systems for novel calculation techniques.

Challenge 3: Different coincident processes take place on multiple time scales in a catalyst system. When looking at OER catalysts, there are several factors which are worth investigating by *operando* experiments to enable the understanding and the evaluation of the whole catalytic system:

(1) the metal (oxide) based active center, which can be inhomogeneous,
(2) possible coexistence of inactive phases,
(3) the support,
(4) the intermediates and precursors for O_2 formation,
(5) the O_2 gas bubbles which form, grow and detach from the electrode,
(6) the solvent, here water, which is also a reactant,
(7) the ions in solution,

This journal is © the Owner Societies 2023

Phys. Chem. Chem. Phys., 2023, **25**, 26958–26971 | **26959**

(8) possible dopants in the solid, and

(9) impurities.

All of them are involved in the reaction to some extent, and several processes happen in parallel, but on different length and time scales.

Electron transfer itself occurs on the sub ps time scale. Solvent reorganisation and relaxation *via* vibrational modes occurs typically on a time scale of several hundred picoseconds. In electrochemical systems, charging and discharging of the double layer capacitance makes the intrinsic time scale externally accessible *via* electrochemical experiments, typically μs and above. Time scales for transport processes to and from the electrode depend on convection. Bubble detachment occurs on the s time scale, and affects convection. Catalyst or support degradation is typically the slowest process for an industrially relevant catalyst, where it happens on the time scale of years. A well designed *operando* experiment must try to maximize the impact of the process of interest on the measured signal, while diminishing the influence of the other processes. Unfortunately, it is not always obvious which process is the easiest to capture in a particular experiment. Particularly challenging are usually the slowest and the fastest processes. Depending on the turnover frequencies, the lifetime and the rate limiting step, the active center of the catalyst may be 'invisible' due to the relatively long time frame necessary for *in situ* data collection.[25] Thus the dominating observed state is not necessarily the active state.

Challenge 4: Observations depend on the electrochemical protocol, as time and potential-dependent processes may be intertwined. Typical *operando* spectroelectrochemical experiments employ chronoamperometric or chronopotentiometric protocols – both with interleaved potential or current steps–, or linear sweep experiments. Especially with linear sweep or other potentiodynamic protocols, time dependent processes, such as surface changes or diffusion processes, are probed entangled with the potential dependent processes. The nature *e.g.* of nucleation processes can lead to substantially different responses under these different protocols. To disentangle these processes different protocols must be applied and varied and analysed in detail. However, not all *operando* methods are compatible with the required different electrochemical protocols, potentially limiting the level of insight which can be obtained. Generally, the history of a system may affect its future behaviour, which must be considered in the choice of the electrochemical protocol.

Challenge 5: Sample requirements of *operando* setups. Each *in situ* or *operando* technique has specific sample requirements and methodical limitations that must be taken into account to obtain meaningful results. These limitations usually do not allow studying an electrocatalytic system under conditions relevant to an industrial environment. For instance, often the sample must have certain optical or structural properties, electrolyte concentrations must be moderate, gas formation must be minimized or long time high currents must be avoided. Thus, model systems are usually studied which are designed to still be sufficiently close in all aspects to an application-relevant

electrocatalyst, but on the other hand simple enough to be accessible to a variety of techniques. Finally, the model should also allow a transfer of the results back to the more complex system for an advancement.

Challenge 6: Intense irradiation may damage the samples. The high energies or intensities used in some spectroscopic techniques may lead to irreversible changes in the sample structure, which are not always easily deduced or may lead to false conclusions. As discussed below, especially X-ray absorption and emission as well as laser based techniques such as Raman spectroscopy may cause sample damage. As a consequence, a critical analysis of the experimental results is required, considering the influence of possible sample modification.

Challenge 7: Many *operando* methods are not surface specific. Catalysis occurs at the interface between electrolyte and the catalyst where the active centers can access the reactants. In almost all practically relevant cases the surfaces are not ideally bulk terminated but rather transformed due to a variety of processes.[26] Underneath the reconstructed surface a significant amount of non-active bulk material can be present. This bulk may give a signal much higher than the species of interest at the interface due to the lack of an intrinsic surface specificity of most *operando* techniques. This covering effect is further amplified by the naturally short life time of the catalytically active centers. In the worst case, the catalytically inactive bulk still shows redox behaviour that is not related to the catalytic activity but masks the changes of interest.

2.2 Specific challenges of Mn oxides

Challenge 8: The dissolution of Mn competes with the OER at practically relevant currents. The potential-pH diagram in Fig. 1 helps to illustrate some of the particular challenges of the Mn system. With reference to the active center in PSII it is worth noting that the presence of Ca^{2+} for activities up to 1 does not change the diagram when neglecting mixed Ca Mn oxides and relying only on the intrinsic databases of the MEDUSA software used to calculate this diagram.[27] Obviously, over a large pH-range MnO_2 is the stable phase around the line indicating the beginning of oxygen evolution. However, with increasing pH, the oxygen line approaches the line indicating oxidation of MnO_2 to MnO_4^-, *i.e.* the transpassive dissolution of Mn and its oxides. Taking into account the solubility of the formed oxides and hydroxides in water (coloured areas in Fig. 1), Pourbaix ranked metals by their "practical nobility" with Mn being placed 43rd of 43 ranked elements. Other metals with oxides catalyzing the OER would be for instance Ru and Ir which are among the top 10 and Ni and Co which rank at 29 and 30 in this scale.[28]

An interesting feature of MnO_x is that a region of limited stability exists at lower pH above the OER potential. This region makes MnO_x particularly interesting for applications as an OER catalyst in photoelectrochemical cell devices (aka 'artificial leaves') at low currents in acidic to neutral pH.[17,29,30] However, the dissolution of Mn oxides at elevated pH and currents is a major challenge for the applicability of such systems in industrial alkaline water electrolyzers or PEM electrolysis cells.[11,31–33]

26960 | *Phys. Chem. Chem. Phys.*, 2023, **25**, 26958–26971

This journal is © the Owner Societies 2023
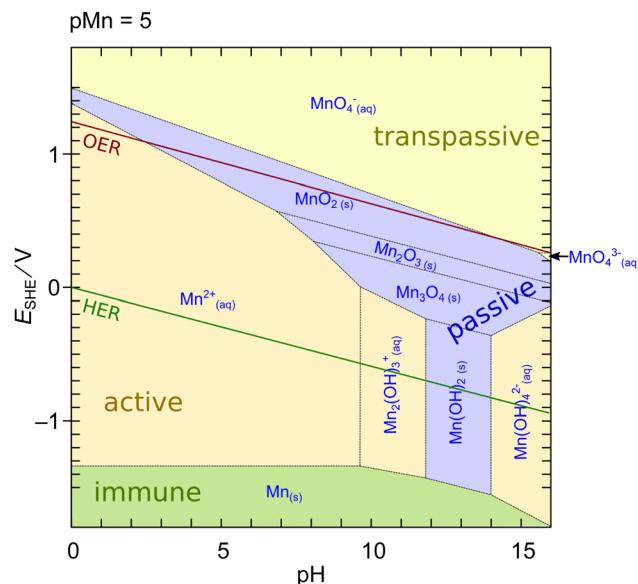
Fig. 1 Potential–pH (Pourbaix) diagram of Mn calculated using MEDUSA[27] at an activity of dissolved species of 10^{-5}. Shading color of the areas refers to the water solubility of the respective phase: green – insoluble metal; blue – insoluble oxide/hydroxide, yellow – soluble ion. Red and green lines indicate oxidation/reduction potentials of water to molecular oxygen and hydrogen, respectively.

The dissolution issue on the other hand implies that experimentally measured currents at elevated potentials often do not exclusively originate from oxygen evolution. In contrast, a purely thermodynamical reasoning is insufficient because the actual rate of dissolution is defined by the kinetics of the reactions which can be sluggish.[26,33] Furthermore, the diagram in Fig. 1 may change in the presence of further ions or compounds which can significantly change the thermodynamics or kinetics of the dissolution.

Challenge 9: Even *ex situ* it can be difficult to determine the oxidation state of Mn unambiguously. The variety of stable Mn oxidation states and the possibility of their coexistence in one sample can make an unambiguous experimental determination difficult. Solid phases exist for at least three oxidation states: Mn^{II}, Mn^{III} and Mn^{IV} (Fig. 1). Mn^{VII} exists as soluble species at high potentials. Especially in alkaline solution, Mn^{V} and Mn^{VI} also exist as intermediates,[34] and there is no reason to exclude their existence in a solid phase.

Challenge 10: In addition to the variety of oxidation states, MnO_x form many different polymorphic forms. Each of these

polymorphs has its own intrinsic defect chemistry and in particular also the possibility to include Mn atoms in lower oxidation states. The latter is correlated with the amount and charge of metal ions in the tunnels or interlayer regions.[35,36] More than 30 Mn oxide and hydroxide minerals exist. The ones mentioned in this paper are listed with their structural properties in Table 1. The structure of many of these oxides can be understood as chains of edge- or corner-sharing MnO_6 octahedra forming tunnel or layer structures as exemplified in Fig. 2.

On the one hand, this diversity makes MnO_x interesting as potential catalysts.[5] On the other hand, this heterogeneity makes fundamental studies, isolating individual aspects of a more complex problem, extremely difficult. An electrocatalyst prepared under certain conditions is likely to transform at elevated electrode potentials so that the actual catalytically active phase differs from the initially prepared material.

While all the features of the Mn oxide systems described above make a full interpretation of *operando* spectroscopic data challenging, they also highlight the strong need for studying such systems both "in situ" and "operando". As one electrochemistry textbook puts it: "*It cannot be over-emphasised how important it is to study any electrode process by as wide a variety of techniques as possible; only by this means can a reliable picture of the reaction be built up*".[37]

In the following, the specific basics for several important experimental methods shall briefly be highlighted and their recent application to Mn-based electrocatalyst systems shall be described, together with a critical analysis of the obtained results.

3. *Operando* studies of Mn oxide based systems during the OER

3.1 Vibrational spectroscopy

Vibrational spectroscopies, especially *operando* Raman spectroscopy, can yield information on the chemical identity of catalytically active materials. General introductions into the basic principles of these methods are available elsewhere.[38–40] For an interpretation of the obtained spectra, thorough knowledge of the important vibrational modes of the bulk system is often required. To that end, several systematic studies of different common Mn oxides with X-ray diffraction based structural characterisation are available.[41–48] Despite the many efforts to bring order into the vast variety of Mn oxide Raman spectra, the

Table 1 MnO_x-compounds discussed in this work

Mineral (compound)	Ideal chemical formula	Tunnel/layer structure
Hausmannite	$Mn^{II}Mn^{III}_2O_4$	Spinel-like
Hollandite group (α-MnO_2)	$R_{0.8-1.5}(Mn^{IV}, Mn^{III})_8O_{16}$ R = Ba, Pb, K or Na	2×2 tunnel
Pyrolusite (β-MnO_2)	$Mn^{IV}O_2$	1×1 tunnel
Romanechite	$Ba(Mn^{IV}, Mn^{III})_5O_{10} \cdot 2H_2O$	2×3 tunnel
Birnessite group (δ-MnO_2)	$(Na, Ca, K)(Mn^{IV}, Mn^{III})_2O_4 \cdot 1.5H_2O$	Layered
Bixbyite	$(Mn^{III})_2O_3$	

This journal is © the Owner Societies 2023

*Phys. Chem. Chem. Phys.*, 2023, **25**, 26958–26971 | **26961**
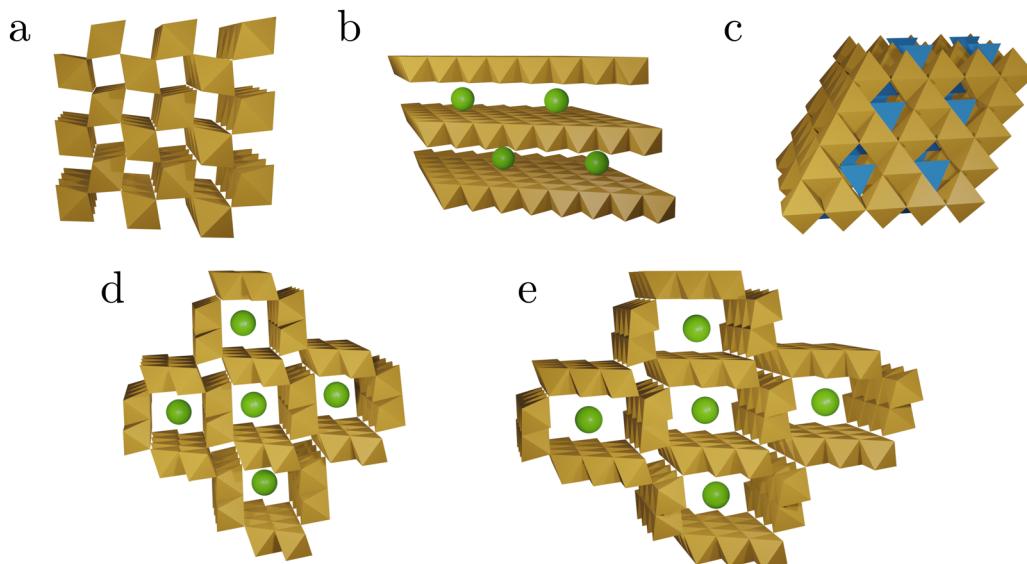
Fig. 2 Schematic representations of the tunnel and layer structures in MnO_x discussed in this work. The structures shown consist of MnO_6 octahedra (brown), MnO_4 tetrahedra (blue), and spheres representing other cations or water (green). Structural details are listed in Table 1. Pyrolusite, β-MnO_2 (a), birnessite δ-MnO_2 (b), spinel structure (c), hollandite α-MnO_2 (d), and romanechite (e).
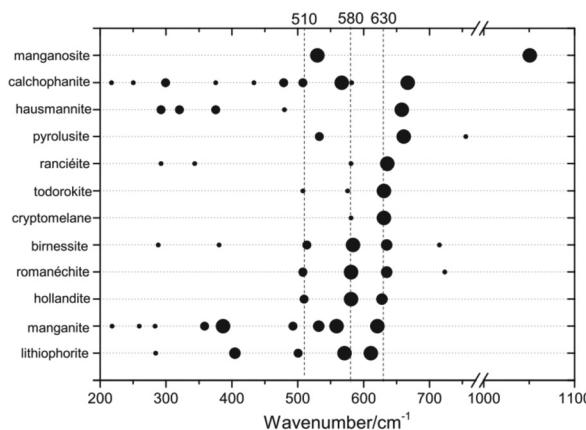

Fig. 3 Raman band positions of selected MnO_x. The dot size is proportional to the observed band intensities. Figure reprinted from ref. 41 with permission. Copyright 2019 John Wiley & Sons, Ltd.

reference spectra in the literature remain contradictory and confusing. A recent study provides an extensive and systematic collection of natural Mn oxides and addressed several contradictions and conflicts in the literature of recent years.[41] Especially, the thermal instability of some MnO_x may have led to contradicting results in the study of reference materials (Challenge 6).

The dominating Mn oxide vibrational modes are between 200 and 750 cm^{-1} (Fig. 3), which is easily accessible using standard lab-based Raman spectroscopy. Many $Mn^{II,III,IV}$ oxides that may be of interest for OER catalysis, give rise to pronounced Raman modes above 500 cm^{-1}, which result from the symmetry of the structure. A mode around 510 cm^{-1} has strong contributions from Mn–O–Mn deformation, while the typically most intense modes around 580 and 630 cm^{-1} have strong

contributions from Mn–O bond stretching.[41,44] For the latter it was shown that the position of these prominent 'marker modes' depends on the average Mn–O distance and the polymerisation of the framework, *i.e.*, the number of shared edges between the MnO_6 octahedra. This useful structural correlation was employed in the interpretation of Raman spectra of MnO_x OER catalysts.[32,49–51]

On the other hand, the strong similarities between spectra of different MnO_x phases above 500 cm^{-1} can make a unique identification of a particular oxide extremely difficult, especially in mixed and dynamic systems as generally found for OER electrocatalysts. For instance, the patterns observed *in situ* during electrochemical oxidation of metallic Mn have been identified as α-MnO_2,[32] based on the similarity to reference spectra.[44] Very similar spectral features have otherwise been assigned to the birnessite like phase prepared by electrochemical deposition[50] based on previous XAS results.[52] Indeed, from a recent extensive analysis of spectra of well-defined compounds, it was concluded that it is virtually impossible to make a clear distinction between hollandite (α-MnO_2), birnessite (δ-MnO_2) and romanechite on the basis of Raman data alone.[41]

The OER performance of differently prepared hollandite α-MnO_2 materials (aka cryptomelane) was studied.[53] Differences in the electrochemical OER performances of the different materials were found to mainly be governed by differences in conductivity originating from morphological differences. However, the initially good electrochemical OER performance of the materials degraded quickly over time. *Operando* Raman spectroscopy yielded remarkably stable spectra during the OER revealing no significant transformations in the materials, thus the reasons for the activity loss remained indistinct. It appears unlikely that the materials do not change when simultaneously a deactivation is observed. This illustrates a specific challenge

26962 | *Phys. Chem. Chem. Phys.*, 2023, **25**, 26958–26971

This journal is © the Owner Societies 2023

for Raman spectroscopy, which is that the Raman cross-sections of different species differ significantly. Consequently, it is hard to get a representative picture of the surface species. Hence, quantitative information about the relative concentration of the species cannot be obtained and some species might even be virtually invisible in the Raman spectra. Furthermore, Raman spectroscopy is not *per se* surface specific (Challenge 7), however several strategies can be used to circumvent this problem.

Thin oxide layers of a few nm thickness on a Raman inactive substrate can be a workaround for the lack of surface specificity. To that end, electrochemically oxidized metals have been studied during the OER.[32] The thicknesses of the formed oxide layers were below 10 nm, but Raman *in situ* measurements showed that the oxide layers remained intrinsically stable during voltammetric sweeps, down to relatively low potentials. During oxygen evolution the Raman spectra did not show similarities to any isolated stable oxide. Also, the spectrum shared some similarities with β-MnO_2, but also distinct differences. Very broad bands around 600 cm^{-1}, assigned to the Mn–O stretching vibrations showed that a strongly disordered MnO_2 was present during the OER. The occurrence of the stretching vibration at this position indicates that the disordered oxide is structurally based on the octahedral coordination of Mn.

For well characterised materials the specific synthesis of reference compounds for the assignment of Raman bands can be very helpful. For instance, *operando* Raman spectroscopy was used to study a selection of MnO_x based catalysts, prepared by electrodeposition on ITO working electrodes.[50] The oxide layers featured thicknesses up to 300 nm and the two (out of three) catalysts with the higher onset potentials underwent structural changes in the pre-OER region, attributed to a charging process. Comparison of the observed spectral changes with spectra of well defined birnessite structures led to the conclusion that charging includes a transformation from tri-clinic to hexagonal Birnessite and the formation of point defects. It was concluded that the formation of an amorphized birnessite structure and bixbyite-like Mn^{III} centers facilitated the OER.[50]

Alkali-metal manganese borophosphates were prepared using a mild-hydrothermal method and showed promising OER performances and stabilities.[54] A thorough *ex situ* characterisation in combination with *in situ* Raman spectroscopy showed that these materials just served as pre-catalysts. Under OER conditions another active phase was formed which was termed a-δ-MnO_2. It was described as being amorphous with a short range order similar to birnessite which was concluded from comparison of the Raman spectra with literature. It was concluded that during the oxygen evolution, corrosion of the pre-catalysts took place, forming a-δ-MnO_2 while dissolving boron and phosphate species and incorporating potassium from the electrolyte. The leaching led to an increasing porosity of the materials which was assigned to the improved OER performance.

Using surface or tip enhanced Raman spectroscopy (SERS or TERS, respectively) can make Raman spectroscopy sensitive to sub-monolayer coverages. For instance the reduction of MnO_2

and reoxidation of $Mn(OH)_2$ was studied in an early application of *in situ* SERS.[55]

Thin MnO_x OER catalyst films were prepared on SERS active substrates by RF-magnetron sputtering.[51,56] The variation in the oxygen content in the sputter gas allowed for control of the Mn/O ratio in the final film, yielding samples, which were mainly made up of MnO_x in the main oxidation states II, III and IV. Here, only the samples in the main oxidation states II and IV are discussed, since they are the most representative. In the atmosphere, films with low O content (termed Mn(II)) were easily oxidized and readily decomposed under laser irradiation, while the stable, higher oxidized MnO_x phases (termed Mn(IV)) consisted of mixtures of different Mn oxides with an average oxidation number of 3.7–3.8 which was also supported by XPS studies. The *operando* Raman spectra indicated that Mn(II) samples (Fig. 4a and b) were oxidized when approaching the OER, showing spectra similar to the Mn(IV) samples (Fig. 4c and d) which also indicated the formation of catalytically active Mn^{III}. For the Mn(IV) phase a slight blue shift of the A_g(2) mode (from 667 to 681 cm^{-1}) and a red shift of the main Mn–O stretching band (from 599 to 568 cm^{-1}) was found during the OER as well as a signal appearing at 503 cm^{-1} and shifting to 479 cm^{-1} at higher potentials. This was interpreted as being due to the formation of additional Mn^{III} species and to an increase in the interplanar spacing between MnO_6 octahedra, which could allow additional inclusion of potassium ions and water in the formed tunnel and/or layer structures. The shape of the signals and their potential dependent behaviour was found to be very similar to the Raman results of mixed Birnessite/Bixbiyte phases in ref. 50. The origins of
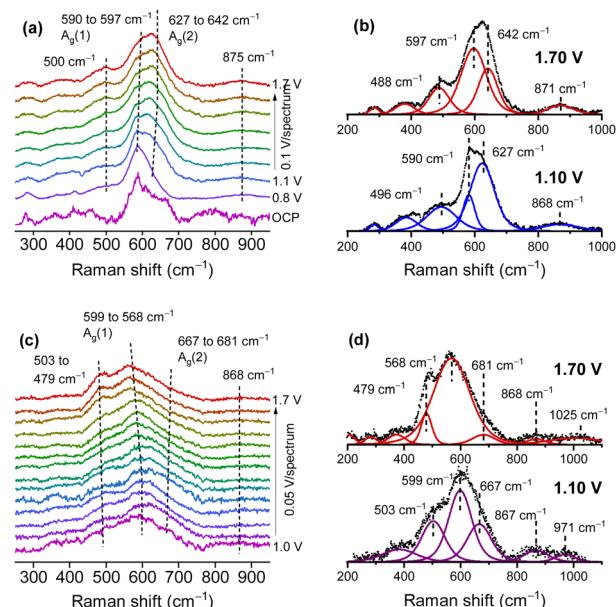

Fig. 4 *Operando* Raman spectra of the Mn(II) (a) and (b) and Mn(IV) (c) and (d) phase in 0.1 M KOH. Fitted spectra (b) and (d) at two selected potentials below and above the oxygen evolution potential. Potentials are *vs.* the reversible hydrogen electrode (RHE). Figure adapted from ref. 56 under CC BY 4.0 license.

This journal is © the Owner Societies 2023

Phys. Chem. Chem. Phys., 2023, **25**, 26958–26971 | **26963**

different peaks in the region close to and above 850 cm^{-1} that were observed in the OER active MnO$_x$ ref. 32 and 51 (*cf.* Fig. 4) remain a matter of speculation. In fact, spectra of natural reference materials scarcely show peaks in this region, for instance a mode around 840–850 cm^{-1} was found only occasionally in reference spectra of β-MnO$_2$.[41,42,45,47] The formation of peroxo species maybe a possible origin of such peaks.[57] An alternative explanation may be the excitation of multi-phonon modes or combination modes which significantly increase in intensity because of symmetry breaking in the presence of certain defects included in the defect rich films during the OER.

Note added in proof: During peer review, the question arose if the Raman spectra show any dependence on the excitation laser wavelength used. Such effects are indeed an important further aspect which could complicate *operando* Raman analysis and data interpretation. In this system excitation wavelength dependence could arise from (a) heat-induced or photochemical damage, (b) selective resonance enhancement of certain features, or (c) complex solid state phenomena. Manganese oxides are very well known to show transformations upon intense illumination, as documented systematically, *e.g.*, in ref. 41. Some earlier studies may have been affected by such transformation. As transformations are typically induced by local heating upon, heating is affected by light absorption, which is strongly wavelength dependent. Hence illumination thresholds are very likely different for different excitation wavelengths. Resonance enhancement of certain features may or may not account for differences observed when comparing spectra with UV excitation to spectra with 633 nm excitation.[41] However, a systematic understanding of such effects is according to our knowledge lacking. Specific phenomena in solids can also lead, *e.g.*, to wavelength dependence of peak positions. A prominent example is the D band in sp^2 carbon systems, which shifts systematically with excitation wavelength because of a Kohn anomaly.[58] Such shifts have to our knowledge not been reported in literature for relevant manganese oxides. The conditions during OER and the nature of transient species make it difficult to rule out such phenomena, and to study them systematically.

3.2 UV/Vis absorption and photoluminescence

Mn^{III} and Mn^{IV} containing oxides are typically brown to black in colour, *i.e.* they have a strong light absorption in the visible spectrum. While on the one hand, black substances are difficult to characterise by absorption spectroscopy, their strong optical absorption also implies that absorption spectroscopy and possible photoluminescence (PL) as a follow up process is a sensitive tool to detect them. The use of UV/Vis absorption, but also PL spectroscopy, for *operando* characterisation has been described by some of us recently.[39]

Mn^{IV} oxides typically have a small bandgap of 1–2 eV.[59] Consequently, UV/Vis absorption spectroscopy can be used to analyse the electronic structure around the band gap, and the presence of intragap states indicative of defects. For instance the local environment of Mn^{III} in a reduced, activated MnO$_2$ catalyst was modeled by oxidizing Mn^{II,III} in a hausmannite like
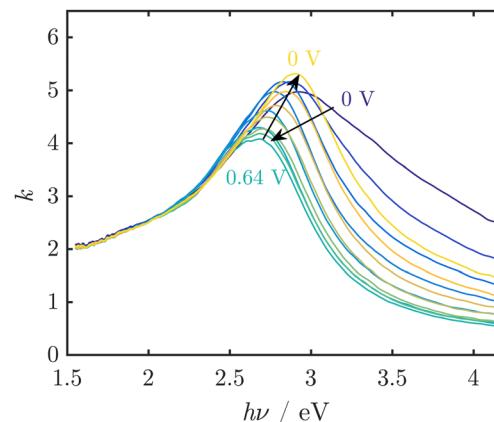

Fig. 5 UV/Vis spectra of thin MnO$_x$ films, represented by the imaginary part k of the complex refractive index, at pH 13 during electrochemical cycling show reversible peak shifts. In this example, the OER onset was observed at ≈ 0.55 V *vs.* Ag/AgCl/3 M KCl. Figure adapted from ref. 32 under CC BY 3.0 license.

(α-Mn$_3$O$_4$) structure to Mn^{III,IV}.[49] The authors found significantly lowered energy gaps between the highest occupied molecule orbital (HOMO) dominated by O 2p and the lowest unoccupied MO (LUMO) originating from antibonding states from tetrahedrally coordinated Mn^{III}. The reduced gap can facilitate the formation of oxygen holes, *i.e.* reactive oxyl radicals as intermediates. Reduced HOMO–LUMO gaps should manifest in a measurable red shift in the UV/Vis absorbance.

Spectroscopic ellipsometry was employed to obtain spectra of MnO$_x$ thin films, which showed reversible red shifts in potential regions before the OER sets in and during the OER (Fig. 5).[32] However, the observed spectral shapes are not well understood and could not be easily interpreted on the basis of the spectra of known oxides (Challenge 2). The observed peaks cannot be explained by the commonly reported absorption spectra of crystalline MnO$_x$. Hence, the occurrence of broad peaks in the region around where the band gap is expected implied a complex defect chemistry inducing states in the gap, but also modifying significantly the density of states just below the valence band level or just above the conduction band level. Thus, it was concluded that the active MnO$_x$ consists of a defect rich, disordered MnO$_2$.

Also the bifunctionality, *i.e.* the ability to catalyse both the OER and ORR, of MnO$_x$ catalysts has been studied. These catalysts are specifically interesting for reversible applications such as rechargeable metal–air batteries or regenerative fuel cells.[60] An Mn$_2$O$_3$ bifunctional catalyst was studied by *in situ* UV/Vis/nIR spectroscopy and *ex situ* PL spectroscopy.[61] To that end, characteristic emissions from electronic transitions of various cationic defects were assigned to the observed PL spectra in the nIR, which was further supported by reference spectra. The bifunctional catalyst featured a reversible polarity switch from p-type to n-type between OER and ORR potentials as determined by electrochemical impedance spectroscopy and Mott–Schottky analysis. The spectroscopic results indicated that the two different states were caused by formation of Mn^{IV}, Mn^{V} high valence and Mn^{II} low valence states, respectively.

26964 | *Phys. Chem. Chem. Phys.*, 2023, **25**, 26958–26971

This journal is © the Owner Societies 2023

Interestingly, *ex situ* PL recorded with a confocal micro Raman setup indicated that the changes occurred in the material surface only, not in the bulk. The surface-only nature of the modification was explained by the structure of bixbyite α-Mn_2O_3 which, unlike many other MnO_x with tunnel or layer structures, has no major voids allowing –OH ion insertion in the bulk material during the OER and ORR. The high and low valence states were proposed to act as the catalytic centers during the OER and ORR, enabled by the low defect formation potentials.

The pH dependency of the OER activity of δ-MnO_2 nanoparticles (potassium birnessite) was examined by *operando* UV/Vis absorption spectroscopy.[62] In particular the OER onset with this catalyst had an increasing overpotential η in the pH range 4–8 and a decreasing η for pH >9, indicating different mechanisms in these regions. A reversible absorption peak that showed a similar pH dependency was found at 510 nm but could not be assigned based on existing literature (*cf.* Challenge 2). Therefore, an assignment to Mn^{III} was based on comparison experiments using pyrophosphate as a probe. The Mn^{III} is assumed to be a precursor for O_2 evolution and the observed higher η at pH <9 is thus a result of Mn^{III} instability because of disproportionation. However at pH >9, Mn^{III} can be generated by conproportionation leading to a decreasing η. Following up on these results the authors were able to significantly reduce η at pH 8 by means of an amine containing polymer.[63] Also here *in situ* UV/Vis spectroscopy substantiated that stabilisation of surface Mn^{III} caused this effect. For the same catalyst an additional blue shifted absorption peak at 470 nm appeared under OER conditions at elevated pH was reported later.[64] The shift was explained by deprotonation of surface specific Mn^{III} species. Accumulation of protons was shown to vary the ratio of the two absorbance peaks and was correlated with the OER current. Due to missing reference spectra (Challenge 2) the exact Mn^{III} species could not be determined unequivocally, but the authors argued for the formation of Mn^{III}–O^- at basic and of Mn^{III}–OH at neutral to acidic pH.

3.3 X-Ray spectroscopy

At higher photon energies, X-ray spectroscopy is a powerful tool to elucidate the core level electronic structure of a material on an atomic level. The theory of these methods and their applications to water oxidation catalysts in general have been extensively reviewed recently.[65,66] Both X-ray absorption spectroscopy (XAS) and X-ray emission spectroscopy (XES) are frequently used techniques. Absorbance of X-ray photons leads to edge features in the spectra. Their position depends on the energy level of the excited core electrons. Therefore, 3d transition metal K-edges are located in the hard X-ray regime (5–10 keV), while oxygen K-edges and metal L-edges are observed in the soft X-ray regime (400–1200 eV).

XES experiments monitor the fluorescence relaxation process after ionization. They are greatly limited by the effective solid angle of detection imposed by the spectrometer. Therefore, these experiments remain very challenging for electrochemical *operando* studies and to the best of our knowledge

to date there have been only a few examples of *operando* spectroelectochemical XES on Mn, both in the soft and hard X-ray regime.[67–70] For a non-ionizing excitation into an intermediate (previously unoccupied) electronic state, the emission experiment becomes resonant and is referred to as resonant XES (RXES) or resonant inelastic X-ray scattering (RIXS).

3.3.1 Hard X-ray absorption spectroscopy. An important aspect of hard X-ray spectroelectrochemistry is that, in contrast to XPS which is more surface sensitive, X-rays at typical transition metal K-edge energies penetrate several micrometers into the film (Challenge 7). In addition, *in situ* XAS can induce photoreduction or -oxidation, radiation damage, and solvent ionisation (Challenge 6) that might lead to incorrect interpretation of results. These two points as well as an XAS specific discussion on the difference between the experimental and the electron-transfer time scales (Challenge 3) have been discussed in great detail, earlier and examplified using cobalt oxide OER catalysts.[25]

One of the first *operando* SEC XAS studies at the Mn K-edge was performed on MnO_x catalysts that have been developed to perform both ORRs and OERs at moderate overpotentials.[71,72] XANES and EXAFS identified $Mn_3^{II,III,III}O_4$ (hausmannite) as the phase present during the ORR, and a mixture of a birnessite-like phase and a more reduced phase that probably corresponded to unchanged $Mn_3^{II,III,III}O_4$ under OER conditions (*cf.* Fig. 6). Since the reduced phase represented a small fraction of the sample, it was assumed that the porous structure of the electrocatalyst enabled good electrochemical control and electrolyte access to most of the sample and therefore increased activity.[72]

Dissociation of a tetranuclear Mn cluster into Mn^{II} compounds upon immobilization in a Nafion matrix has been investigated in detail.[73] These compounds became electrochemicaly re-oxidized to form nanoparticles of a disordered $Mn^{III/IV}$ (birnessite resembling) phase, which is catalytically active. Although the study was not exactly performed under *operando* conditions its results demonstrated that structures resembling that of the PSII water oxidation complex are not a requirement for catalytic performance and that complex structures in a non-biological environment may act only as precatalysts.[73]

The effect of Ni addition to a bifunctional $MnNiO_x$ catalyst was studied by *in situ* XAS complemented by an XES method that allowed for simultaneous detection of signals from multiple metal centers, thereby disentangling the redox behaviour of Mn and Ni.[67] The catalyst as prepared consisted of nano-phase separated crystalline Ni rich and Mn rich oxide phases. The presence of Ni resulted in a lower oxidation potential for Mn, facilitating the oxidation towards Mn^{IV} during the OER as compared to the Ni-free catalyst. The $MnNiO_x$ was found to be bifunctional for the ORR and OER. While the oxidation states of Ni and Mn changed upon transition from the ORR to the OER regime, no major structural changes where observed.

Thin films of an MnO_x co-catalyst on a $SrTiO_3$ photoelectrode were studied using *in situ* XAS.[74,75] The results implied UV irradiation and potential dependent slow oxidation of the co-catalyst, from an average Mn oxidation number of +3.1 to

This journal is © the Owner Societies 2023

Phys. Chem. Chem. Phys., 2023, **25**, 26958–26971 | **26965**
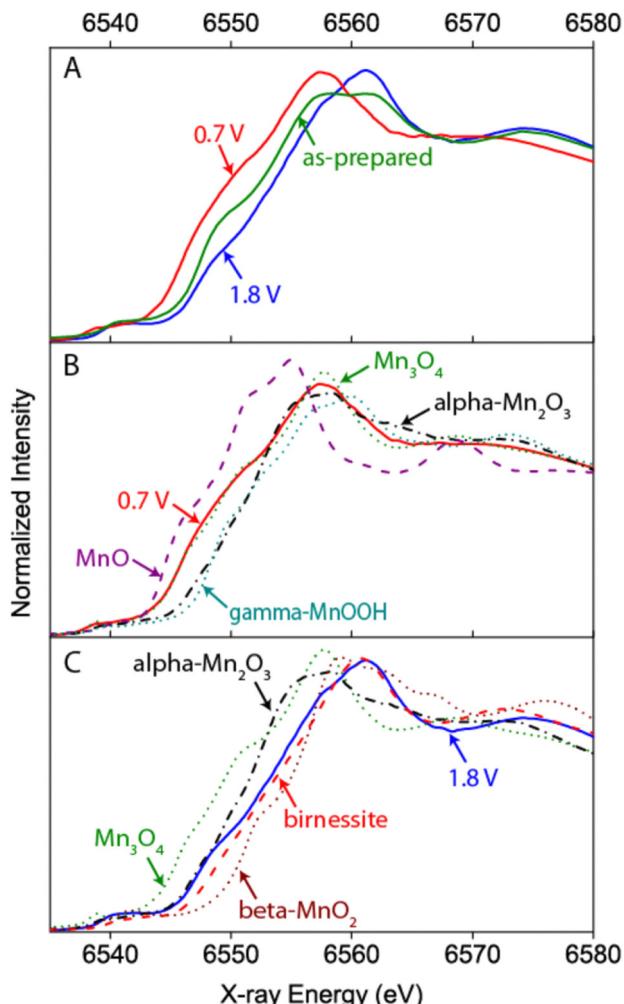
Fig. 6 Example of a hard X-ray study undertaken by Gorlin *et al.* on a MnO_x film prepared on a Au coated Si_3N_4 membrane.[72] The Mn K-edge XANES undergoes clear changes with respect to the "as-prepared" state when ORR or OER conditions are applied indicating a reduction or oxidation of the catalyst, respectively (A). A comparison to spectra of reference samples additionally allows an estimation of the oxidation state and phase composition under the respective conditions (B and C). Reprinted with permission from ref. 72. Copyright 2013 American Chemical Society.

+4 at an applied potential of 1.0 V (RHE) and to +3.3 at 0.5 V (RHE). The irradiation strongly influenced the rate of the oxidation, indicating that oxidation occurred by holes forming as a result of photoexcitation. The correlation found between hole transfer and OER activity was explained by a potential induced upward band bending in the n-type semiconductor that facilitates the charge separation and the hole transfer to the MnO_x co-catalyst. Interestingly, the OER rate did not show strong dependence on the Mn oxidation state, thus it was concluded that both Mn^{III} and Mn^{IV} rich phases can be photoelectrochemically active to catalyse the OER.

In a combined quasi *in situ* and time-resolved *in situ* XAS study the redox behavior of the biological Mn_4Ca oxide cluster and three different birnessite type Mn oxides (with and without Ca) were analyzed.[76] For the quasi *in situ* technique the samples were freeze-quenched after a potential was applied for 3 minutes and subsequently XAS was measured at 20 K. The low measuring temperature can help to minimize photoreduction by the beam and decreases thermal contributions to the EXAFS, which can greatly increase experimental resolution. For the time-resolved experiment, samples were studied at room temperature and the absorption signal was tracked over time at a fixed excitation energy when changing the potential. The results of catalytically active birnessite type MnO_x and Ca containing MnO_x were compared to an inactive MnO_x and the biological OEC of PSII. It was found that the catalytically active birnessite type MnO_x undergoes oxidation and structural changes that share certain features with the OEC. The catalysts comprised metastable Mn^{III} centers at OER potentials which can accumulate oxidizing equivalents (holes) by $Mn^{III} \rightarrow Mn^{IV}$ oxidation coupled to changes in the μ-oxo bridging. Kinetic experiments implied that metal oxidation precedes the O^{2-} oxidation. The inactive MnO_x showed a significantly higher ordered structure than the active one, implying that non-crystalline materials promote the OER because they allow dynamic and flexible oxidation states and structural changes. This dynamic picture of the MnO_x OER catalyst instead of that of a static active center is quite akin to the mechanism of the biological oxygen evolution in the OEC.[76]

Another study at room temperature, also reported shifts in the Mn K-edge position as a function of applied potential. It was observed that electrodeposited δ-MnO_2 birnessite films initially displayed very low electrocatalytic activity that increased upon cycling between −0.4 and +1.1 V *vs.* NHE (at pH 8.0).[49] A continuous shift of the K-edge position towards lower energies with increasing number of cycles indicating an accumulation of Mn^{III} centers, and EXAFS analysis suggested that the activated material comprised a mixture of α-Mn_3O_4 hausmannite-like and δ-MnO_2 (birnessite) structures in a mixed oxidation state containing Mn^{III} and Mn^{IV}. The authors proposed that all octahedral (O_h) sites contain Mn^{IV}, while Mn^{III} centers remain metastable, kinetically locked in tetrahedral (T_d) sites, unable to disproportionate. A computational model, describing the resulting electronic structure around these $Mn^{III}(T_d)$, features a HOMO dominated by oxygen 2p valence states and a metal-based LUMO with a reduced energy gap as compared to pure δ-MnO_2. Oxidation would create oxygen holes leading to the formation of a very reactive oxyl radical that would explain the enhanced activity of these Mn^{III} containing materials.[49]

The co-deposition of gold particles (2–3 nm diameter) on MnO_x OER catalysis, studied by *operando* XAS, resulted in an increased oxidation state of the MnO_x catalyst under OER conditions compared to a MnO_x without Au particles.[77] The increased oxidation state may have been related to the observed increase in OER activity caused by the gold particles.

An *operando* hard, tender, and soft XAS study was performed on a layered MnO_x catalyst with intercalated potassium ions in an KOH containing aqueous phosphate buffer solution (pH 8).[78] In agreement with the previously discussed studies, the Mn K-edge position shifted to higher energies with increasing potential, indicating a reversible increase of the average oxidation state from ∼+3.1 to ∼+3.9. The shape of the Mn

26966 | *Phys. Chem. Chem. Phys.*, 2023, **25**, 26958–26971

This journal is © the Owner Societies 2023

K-edge spectra and soft X-ray O K-edge spectra resembled δ-MnO$_2$. The catalytic activity of the MnO$_x$ film was attributed to the remaining Mn^{III} species at high potentials. Complementary XAS with tender X-rays at the K K-edge suggested the formation of buserite – the hydrated form of birnessite – under *in situ* conditions.

3.3.2 Soft X-ray absorption spectroscopy and resonant inelastic X-ray scattering. Soft X-ray photon absorption excites 2p core electrons of the 3d-transition-metal centers and yields the L-edge spectra (Fig. 7). These excitations provide access to information about the valence electronic structure, which is involved in chemical bonding and is consequently critical for catalytic processes. Furthermore, with soft XAS, oxygen K-edge spectra can be obtained providing a second handle in the analysis of *e.g.* Mn oxides. The information accessible with soft X-ray comprises band/state energies, energies of electronic transitions, oxidation states, and information about the local coordination environment.

However, the *operando* application of soft X-ray spectroscopy comes with some additional challenges.[79–81] In contrast to

experiments in the visible or hard X-ray regime, the propagation of soft X-rays requires vacuum conditions and the penetration depth of the X-ray photons is limited to a few hundred nanometres. Its limited penetration makes the application of this technique rather challenging for *operando* experiments, in particular because the catalyst needs to be in contact with both the liquid electrolyte and an electrode support to apply a potential. This experimental challenge might be one reason why *operando* soft X-ray spectroscopy studies are still exceptional compared to hard X-ray experiments. In addition, the emission intensity of soft X-ray photons during the 3d2d-relaxation processes is rather low and photon yield experiments have to be conducted very thoroughly to avoid radiation induced changes of oxidation states or radiolysis of the electrolyte (Challenge 6). Nevertheless, during the past few years several *in situ/operando* studies with soft X-rays have demonstrated their value for the interpretation of Mn based water oxidation catalysts.

A combined absorption/emission study, complemented by *operando* total electron yield and combined with modeling,
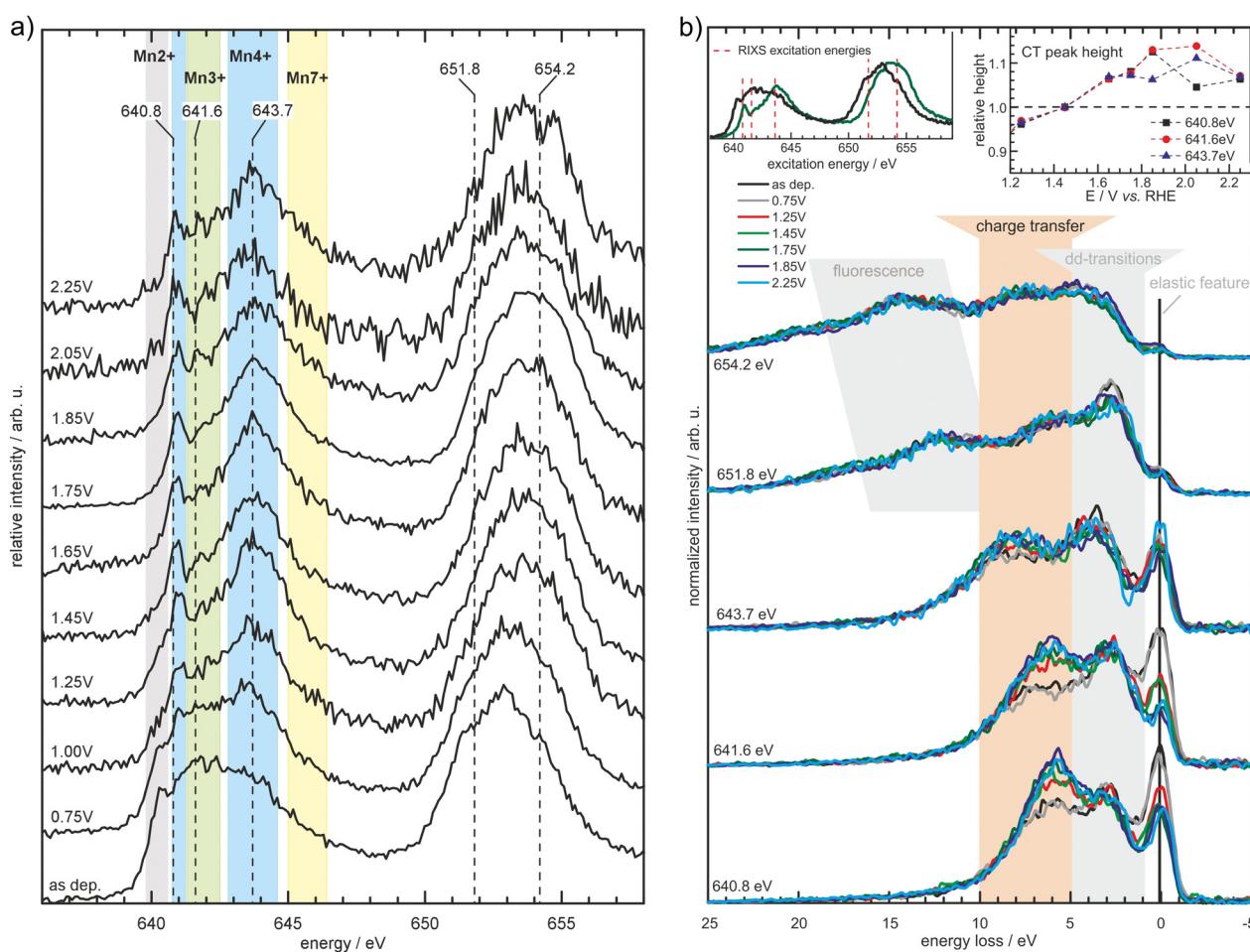

Fig. 7 Partial fluorescence yield spectra measured at the Mn L$_{2,3}$-edges (a) for MnO$_x$ in borate buffer (0.1 M, pH 9.2) at the specified potentials (*vs.* RHE). The spectral shape changes depending on the applied potential with the background shading indicating spectral regions where particular Mn oxidation states typically exhibit prominent features. Further results obtained by inelastic X-ray scattering (b) measured at the excitation energies depicted in (a) and the left inset of (b) reveal further potential induced changes in the electronic structure of the MnO$_x$-catalyst, manifesting itself as a decrease of the elastic feature and increase in the charge transfer feature (highlighted by the orange background shading and the right inset). Reprinted with permission from ref. 68. Copyright 2019 Wiley-VCH Verlag GmbH & Co. KGaA, Weinheim.

This journal is © the Owner Societies 2023

Phys. Chem. Chem. Phys., 2023, **25**, 26958–26971 | **26967**

was undertaken on an electrodeposited MnO_x thin film for the OER applied in 0.1 M borate buffer (pH 9.2).[68] It was shown that δ-MnO_2 (birnessite) is the main stable phase at OER conditions and no evidence for Mn in a higher oxidation state than +4 was found. Furthermore, RIXS experiments revealed an increase of a feature that is related to metal–ligand charge transfer (Fig. 7). This was associated with the evolution of the hybridization of Mn–O bonds with increasing potential leading to facilitation of metal–ligand electron transfer and the formation of O^- species.

Mn valency and the role of Mn–O hybridization was studied in detail with a layered Mn oxide catalyst for the ORR and OER, by (inverse) partial fluorescence yield experiments at the Mn L-edges and the O K-edge.[82] The catalyst was an electrodeposited birnessite type film applied in 0.1 M KOH. Upon cycling between ORR and OER conditions, the Mn valence varied between 2.4–2.6 for the ORR with tetrahedral Mn^{II} identified in the sample, and 3.1–3.4 under OER conditions. Analysis of the O K-edge allowed an estimation of the maximum Mn–O hybridization for a Mn valence close to +3 (and an e_g occupancy of nearly one) and the presence of Mn^{III} was suggested to be critical for the OER as well as ORR.

Soft XAS in transmission mode was carried out on an electrodeposited MnO_x film, as a proof of principle to validate the function of a soft X-ray transmission flow cell.[83] Although the authors point out that some of their data may have suffered from radiation-induced damage (Challenge 6) a clear transformation of the Mn L-edge absorption spectrum was observed when increasing the potential from 0.3 to 1.5 V vs. NHE. By using a linear combination fitting approach based on spectra taken on reference materials, the authors disentangle the spectra into contributions of individual MnO_x phases. Decreasing the potential back to 0.3 V showed the hysteretic behavior of the phase transitions. Furthermore, the effect of radiation damage was demonstrated and related to the actual radiation dose during data collection.

The same setup was used to study the oxidation and reduction behavior of a MnO_x thin film electrodeposited in a methylphospate solution and applied for the OER at pH 7 in a KNO_3 containing 0.1 M phosphate buffer solution.[84] Using a linear fitting approach it was found that the freshly prepared films mostly contained MnO_2 (in an oxidation state of +4) with a small amount of birnessite, transforming into a birnessite dominating phase with minor contributions of MnO_2 at 1.5 V vs. NHE. A continuous transformation into birnessite was also observed when activating the film at 1.2 V for 1 h. Subsequent reduction at 0.3 V lead to a decrease of birnessite and an increase of MnO_2 as well as to the formation of Mn_2O_3. No other Mn phases were identified; however, a small mismatch of the fitted data to the recorded spectra was reported (Challenge 2).

A porous layer of MnO_x deposited on a $BiVO_4$ photoanode following a similar deposition and analysis approach, was shown to also transform into a birnessite phase with increasing potential up to 1.91 V vs. RHE.[85] The transformation was facilitated by illumination, attributed to the creation of photogenerated holes in the $BiVO_4$ and subsequent electron

migration. In addition it was found that oxidation of Mn also occurred in this sample system with illumination only.

The influence of Mn loading on Ni catalysts was studied in a Ni L-edge XAS/2p3d-RIXS spectroelectrochemical study.[70] The Mn loaded oxide, Ni_3MnO_4, was compared to pure NiO, and the structure–activity correlations were studied by tracking the changes of the Ni centers before and during the OER. It was found that Mn did not improve the catalytic activity of a pure NiO. Additionally, no significant changes in the electronic structure of the Ni could be identified as a result of adding Mn to the oxide. The study could identify γ-NiOOH as the active phase.

4. Summary and outlook

While the results from the different studies discussed are not free of contradictions, some important common interdependent key features have been extracted for several MnO_x.

I. Disordered structures and structural flexibility. Under working conditions MnO_x are observed that are disordered, amorphous or mixed phases. Furthermore, phases based on octahedral Mn coordination are frequently observed.[32,49,54,72,76,78] In this regard the operando results are consistent with many ex situ studies.[52,73] Several positive influences of the disorder on the OER performance have been discussed. For instance structural defects may kinetically trap metastable intermediates or precursors as proposed for Mn^{III}.[49,62,76] Also, it was argued that non-crystalline materials comprise structural flexibility, allowing structural as well as oxidation state changes during the catalysis,[76] and facilitate charge separation through electron–hole pair formation by reduced energy gaps.[49] Also, the positive influence of flexible μ-oxo bridges in amorphous oxides has been proposed to facilitate redox-potential leveling by coupling μ-OH deprotonation to oxidation steps.[2,76]

II. Flexibility in the oxidation number in the range III–IV. MnO_x found under OER working conditions mostly featured oxidation numbers between +3 and +4. In this regard the MnO_x resemble the biological OEC, where oxidation equivalents are accumulated by redox steps between Mn^{III} and Mn^{IV}. An enhancement of OER activity by the presence of Mn^{III} in MnO_x was also repeatedly reported.[50,54,62,63,76,78] Accordingly, it is assumed that these Mn^{III} act as precursors[62] or constitute the catalytic center.[76] One mechanism was proposed that involved resting states of Mn^{III} centers in acidic environments and mixed $Mn^{III,IV}$ resting states in the alkaline regime.[30] However, OER potentials largely exceed the oxidation of Mn^{III} (cf. Fig. 1). Thus, the structural properties of the catalysts are thought to keep the Mn^{III} centers locally in a metastable state.

III. Activity of birnessite like phases. MnO_x catalysts with as prepared birnessite-like structure have been identified to have good OER activities and thus have been the focus of many studies that used operando methods.[49,50,52,68,76,78,82] Moreover, the formation of additional birnessite phases from other materials under OER conditions or upon catalyst activation has also been observed by operando methods at various pH.[54,68,72,73]

26968 | Phys. Chem. Chem. Phys., 2023, **25**, 26958–26971

This journal is © the Owner Societies 2023

Thus it is possible that other Mn-based materials also convert (partially) into birnessite like structures under OER conditions which can only be probed by *operando* studies. Birnessites, intrinsically unite the properties of the above points I & II. They comprise disordered, layered structures based on edge sharing MnO_6 octahedra, including Mn^{III} and Mn^{IV} centers (Fig. 2b).[35,36] The structural flexibility in birnessites is given by several features. In the interlayer space (distance *ca.* 7 Å) H_2O as well as metal ions can be incorporated and the latter can be easily exchanged.[36] For instance the incorporation of Ca^{2+}, which is essential in biological OER, may be beneficial here. Defects in the MnO_6 layers may act as H_2O coordination sites and missing oxo- or hydroxo-ligands can enable additional μ-O bridges.[86] In contrast, recently the intrinsic OER activity of layered MnO_x has been challenged by the discovery that traces of Ni and Fe ions significantly increase their activity and in the absence of these ions, birnessite's intrinsic OER activity appears to be low.[87]

Despite the challenges outlined in Section 2, *in situ* and *operando* spectroscopy has contributed a great deal to the understanding of reaction mechanisms of Mn-containing electrocatalysts for the OER. A wealth of studies has revealed key features that seem to determine whether a certain Mn material features efficient OER catalysis. Even though the challenges these methods face will not be overcome in the short term, it is hard to imagine progressing our understanding without *operando* spectroscopic analysis. Thus, there is plenty of room for ongoing method development with the existing methods, and also for the application of less widely available techniques. A number of questions remain open, and *operando* spectroscopy may be able to contribute to answering them. For example, the role of and need for the calcium in the biocatalyst, remains at least partly in the dark. Also, the stability issues generally observed at high current densities require further understanding. Stability is without any doubt important for their application, and solving stability issues is crucial for the application of Mn-based electrocatalysts in large scale water splitting applications.

List of abbreviations

EXAFS	Extended X-ray absorption fine structure
HER	Hydrogen evolution reaction
IR	Infrared
nIR	Near infrared
OEC	Oxygen evolving center
OER	Oxygen evolution reaction
ORR	Oxygen reduction reaction
PL	Photo luminescence
PS II	Photo system II
RF	Radio frequency
RHE	Reversible hydrogen electrode
RIXS	Resonant inelastic X-ray scattering
RXES	Resonant X-ray emission spectroscopy
SEC	Spectroelectrochemistry
SERS	Surface enhanced Raman spectroscopy
TERS	Tip enhanced Raman spectroscopy
UV	Ultraviolet
Vis	Visible
XANES	X-Ray absorption near edge spectroscopy
XAS	X-Ray absorbance spectroscopy
XES	X-Ray emission spectroscopy
XPS	X-Ray photoelectron spectroscopy

Conflicts of interest

There are no conflicts to declare.

Acknowledgements

Notes and references

1 K. Kinoshita, *Electrochemical Oxygen Technology*, Wiley, New York, 1992, vol. 1117.

2 H. Dau, C. Limberg, T. Reier, M. Risch, S. Roggan and P. Strasser, *ChemCatChem*, 2010, **2**, 724–761.

3 A. Tanaka, Y. Fukushima and N. Kamiya, *J. Am. Chem. Soc.*, 2017, **139**, 1718–1721.

4 Y. Umena, K. Kawakami, J.-R. Shen and N. Kamiya, *Nature*, 2011, **473**, 55–60.

5 F. A. Armstrong, *Philos. Trans. R. Soc. Lond., B, Biol. Sci.*, 2008, **363**, 1263–1270.

6 D. A. Pantazis, *ACS Catal.*, 2018, **8**, 9477–9507.

7 V. Krewald, M. Retegan, N. Cox, J. Messinger, W. Lubitz, S. DeBeer, F. Neese and D. A. Pantazis, *Chem. Sci.*, 2015, **6**, 1676–1695.

8 J. Yano and V. Yachandra, *Chem. Rev.*, 2014, **114**, 4175–4205.

9 N. Cox, D. A. Pantazis, F. Neese and W. Lubitz, *Acc. Chem. Res.*, 2013, **46**, 1588–1596.

10 P. E. M. Siegbahn, *Acc. Chem. Res.*, 2009, **42**, 1871–1880.

11 J. Melder, P. Bogdanoff, I. Zaharieva, S. Fiechter, H. Dau and P. Kurz, *Z. Phys. Chem.*, 2020, **234**, 925–978.

12 D. B. Wellbeloved, P. M. Craven and J. W. Waudby, *Ullmann's Encyclopedia of Industrial Chemistry*, Wiley-VCH, Weinheim, Germany, 2000, pp. 175–221.

This journal is © the Owner Societies 2023

Phys. Chem. Chem. Phys., 2023, **25**, 26958–26971 | **26969**

13 L. Erdmann, S. Behrendt and M. Feil, *Kritische Rohstoffe für Deutschland*, Institut für Zukunftsstudien und Technologiebewertung/adelphi technical report, 2011.

14 G. Blengini, C. El Latunussa, U. Eynard, C. Torres De Matos, D. Wittmer, K. Georgitzikis, C. Pavel, S. Carrara, L. Mancini, M. Unguru, D. Blagoeva, F. Mathieux and D. Pennington, *Study on the EU's list of critical raw materials (2020): final report*, European Commission and Directorate-General for Internal Market, Industry, Entrepreneurship and SMEs, 2020.

15 B. Kok, B. Forbush and M. McGloin, *Photochem. Photobiol.*, 1970, **11**, 457–475.

16 X. Li, L. Zhao, J. Yu, X. Liu, X. Zhang, H. Liu and W. Zhou, *Nano-Micro Lett.*, 2020, **12**, 131.

17 M. G. Walter, E. L. Warren, J. R. McKone, S. W. Boettcher, Q. Mi, E. A. Santori and N. S. Lewis, *Chem. Rev.*, 2010, **110**, 6446–6473.

18 D. Pletcher and X. Li, *Int. J. Hydrogen Energy*, 2011, **36**, 15089–15104.

19 J. Brauns and T. Turek, *Processes*, 2020, **8**, 248.

20 C. Ros, T. Andreu and J. R. Morante, *J. Mater. Chem. A*, 2020, **8**, 10625–10669.

21 B. M. Weckhuysen, *Chem. Commun.*, 2002, 97–110.

22 M. A. Bañares and I. E. Wachs, *J. Raman Spectrosc.*, 2002, **33**, 359–380.

23 F. Deißenbeck, C. Freysoldt, M. Todorova, J. Neugebauer and S. Wippermann, *Phys. Rev. Lett.*, 2021, **126**, 136803.

24 J.-B. Le, X.-H. Yang, Y.-B. Zhuang, M. Jia and J. Cheng, *J. Phys. Chem. Lett.*, 2021, **12**, 8924–8931.

25 H. J. King, M. Fournier, S. A. Bonke, E. Seeman, M. Chatti, A. N. Jumabekov, B. Johannessen, P. Kappen, A. N. Simonov and R. K. Hocking, *J. Phys. Chem. C*, 2019, **123**, 28533–28549.

26 A. R. Akbashev, *Curr. Opin. Electrochem.*, 2022, **35**, 101095.

27 I. Puigdomenech, Chemical Equilibrium Diagrams, **https://www.kth.se/che/medusa/**, **https://sites.google.com/site/chemdiagr/**, **https://github.com/ignasi-p/eq-diagr/**, 2018.

28 M. Pourbaix, in *Atlas of electrochemical equilibria in aqueous solutions*, ed. M. Pourbaix, National Association of Corrosion Engineers/Centre Belge d'Etude de la Corrosion CEBELCOR, Houston/Bruxelles, 1974, ch. 4-Corrosion, pp. 70–83.

29 M. Huynh, C. Shi, S. J. L. Billinge and D. G. Nocera, *J. Am. Chem. Soc.*, 2015, **137**, 14887–14904.

30 M. Huynh, D. K. Bediako and D. G. Nocera, *J. Am. Chem. Soc.*, 2014, **136**, 6002–6010.

31 F. D. Speck, P. G. Santori, F. Jaouen and S. Cherevko, *J. Phys. Chem. C*, 2019, **123**, 25267–25277.

32 M. Rabe, C. Toparli, Y.-H. Chen, O. Kasian, K. J. J. Mayrhofer and A. Erbe, *Phys. Chem. Chem. Phys.*, 2019, **21**, 10457–10469.

33 J. Peng, L. Giordano, T. C. Davenport and Y. Shao-Horn, *Chem. Mater.*, 2022, **34**, 7774–7787.

34 L. I. Simandi, M. Jaky, C. R. Savage and Z. A. Schelly, *J. Am. Chem. Soc.*, 1985, **107**, 4220–4224.

35 J. E. Post, *Proc. Nat. Acad. Sci. U. S. A.*, 1999, **96**, 3447–3454.

36 Q. Feng, H. Kanoh and K. Ooi, *J. Mater. Chem.*, 1999, **9**, 319–333.

37 C. H. Hamann, A. Hamnett and W. Vielstich, *Electrochemistry*, Wiley-VCH, Weinheim, Germany, 2nd edn, 2007, p. 251.

38 A. Erbe, A. Sarfraz, C. Toparli, K. Schwenzfeier and F. Niu, in *Soft Matter at Aqueous Interfaces*, ed. P. R. Lang and Y. Liu, Springer, Cham, Switzerland, 2016, pp. 459–490.

39 A. Erbe, S. Nayak, Y.-H. Chen, F. Niu, M. Pander, S. Tecklenburg and C. Toparli, in *Encyclopedia of Interfacial Chemistry*, ed. K. Wandelt, Elsevier, Oxford, 2018, pp. 199–219.

40 K. Nakamoto, *Infrared and Raman Spectra of Inorganic and Coordination Compounds: Part A: Theory and Applications in Inorganic Chemistry*, John Wiley & Sons, Inc., Hoboken, NJ, USA, 2008.

41 S. Bernardini, F. Bellatreccia, A. Casanova Municchia, G. Della Ventura and A. Sodo, *J. Raman Spectrosc.*, 2019, **50**, 873–888.

42 C. Julien, M. Massot, S. Rangan, M. Lemal and D. Guyomard, *J. Raman Spectrosc.*, 2002, **33**, 223–228.

43 C. Julien, M. Massot, R. Baddour-Hadjean, S. Franger, S. Bach and J. P. Pereira-Ramos, *Solid State Ionics*, 2003, **159**, 345–356.

44 C. M. Julien, M. Massot and C. Poinsignon, *Spectrochim. Acta A*, 2004, **60**, 689–700.

45 C. Julien, *Solid State Ionics*, 2006, **177**, 11–19.

46 T. Gao, H. Fjellvåg and P. Norby, *Nanotechnology*, 2009, **20**, 055610.

47 T. Gao, H. Fjellvåg and P. Norby, *Anal. Chim. Acta*, 2009, **648**, 235–239.

48 B. Lafuente, R. T. Downs, H. Yang and N. Stone, in *Highlights in Mineralogical Crystallography*, ed. T. Armbruster and R. Danisi, De Gruyter, Berlin, Germany, 2015, ch. The power of databases: the RRUFF project, pp. 1–30.

49 Z. Morgan Chan, D. A. Kitchaev, J. Nelson Weker, C. Schnedermann, K. Lim, G. Ceder, W. Tumas, M. F. Toney and D. G. Nocera, *Proc. Natl. Acad. Sci. U. S. A.*, 2018, **115**, E5261–E5268.

50 H. An, Z. Chen, J. Yang, Z. Feng, X. Wang, F. Fan and C. Li, *J. Catal.*, 2018, **367**, 53–61.

51 H. Radinger, P. Connor, R. Stark, W. Jaegermann and B. Kaiser, *ChemCatChem*, 2021, **13**, 1175–1185.

52 I. Zaharieva, P. Chernev, M. Risch, K. Klingan, M. Kohlhoff, A. Fischer and H. Dau, *Energy Environ. Sci.*, 2012, **5**, 7081–7089.

53 J. Heese-Gärtlein, D. M. Morales, A. Rabe, T. Bredow, W. Schuhmann and M. Behrens, *Chem. – Eur. J.*, 2020, **26**, 12256–12267.

54 P. W. Menezes, C. Walter, B. Chakraborty, J. N. Hausmann, I. Zaharieva, A. Frick, E. Hauff, H. Dau and M. Driess, *Adv. Mater.*, 2021, **33**, 2004098.

55 D. Gosztola and M. J. Weaver, *J. Electroanal. Chem. Interfacial Electrochem.*, 1989, **271**, 141–154.

56 H. Radinger, MSc thesis, Technische Universität Darmstadt, Darmstadt, 2023.

57 K. Nakamoto, *Infrared and Raman Spectra of Inorganic and Coordination Compounds: Part B: Applications in Coordination, Organometallic, and Bioinorganic Chemistry*, John Wiley & Sons, Inc., Hoboken, NJ, USA, 2008, ch. 1.21, pp. 161–175.

26970 | *Phys. Chem. Chem. Phys.*, 2023, **25**, 26958–26971

This journal is © the Owner Societies 2023

58 A. C. Ferrari, *Solid State Commun.*, 2007, **143**, 47–57.

59 D. M. Sherman, *Geochim. Cosmochim. Acta*, 2005, **69**, 3249–3255.

60 J. Pan, X. L. Tian, S. Zaman, Z. Dong, H. Liu, H. S. Park and B. Y. Xia, *Batteries Supercaps*, 2019, **2**, 336–347.

61 I. Roy, Q. Wang and V. Chakrapani, *J. Phys. Chem. C*, 2020, **124**, 5286–5299.

62 T. Takashima, K. Hashimoto and R. Nakamura, *J. Am. Chem. Soc.*, 2012, **134**, 1519–1527.

63 T. Takashima, K. Hashimoto and R. Nakamura, *J. Am. Chem. Soc.*, 2012, **134**, 18153–18156.

64 T. Takashima, A. Yamaguchi, K. Hashimoto, H. Irie and R. Nakamura, *Electrochemistry*, 2014, **82**, 325–327.

65 C. H. M. van Oversteeg, H. Q. Doan, F. M. F. de Groot and T. Cuk, *Chem. Soc. Rev.*, 2017, **46**, 102–125.

66 J. Timoshenko and B. Roldan Cuenya, *Chem. Rev.*, 2021, **121**, 882–961.

67 S. Gul, J. W. D. Ng, R. Alonso-Mori, J. Kern, D. Sokaras, E. Anzenberg, B. Lassalle-Kaiser, Y. Gorlin, T.-C. Weng, P. H. Zwart, J. Z. Zhang, U. Bergmann, V. K. Yachandra, T. F. Jaramillo and J. Yano, *Phys. Chem. Chem. Phys.*, 2015, **17**, 8901–8912.

68 M. F. Tesch, S. A. Bonke, T. E. Jones, M. N. Shaker, J. Xiao, K. Skorupska, R. Mom, J. Melder, P. Kurz, A. Knop-Gericke, R. Schlögl, R. K. Hocking and A. N. Simonov, *Angew. Chem., Int. Ed.*, 2019, **58**, 3426–3432.

69 V. Celorrio, A. S. Leach, H. Huang, S. Hayama, A. Freeman, D. W. Inwood, D. J. Fermin and A. E. Russell, *ACS Catal.*, 2021, **11**, 6431–6439.

70 M. Al Samarai, A. W. Hahn, A. Beheshti Askari, Y.-T. Cui, K. Yamazoe, J. Miyawaki, Y. Harada, O. Rüdiger and S. DeBeer, *ACS Appl. Mater. Interfaces*, 2019, **11**, 38595–38605.

71 Y. Gorlin and T. F. Jaramillo, *J. Am. Chem. Soc.*, 2010, **132**, 13612–13614.

72 Y. Gorlin, B. Lassalle-Kaiser, J. D. Benck, S. Gul, S. M. Webb, V. K. Yachandra, J. Yano and T. F. Jaramillo, *J. Am. Chem. Soc.*, 2013, **135**, 8525–8534.

73 R. K. Hocking, R. Brimblecombe, L.-Y. Chang, A. Singh, M. H. Cheah, C. Glover, W. H. Casey and L. Spiccia, *Nat. Chem.*, 2011, **3**, 461–466.

74 M. Yoshida, T. Yomogida, T. Mineo, K. Nitta, K. Kato, T. Masuda, H. Nitani, H. Abe, S. Takakusagi, T. Uruga, K. Asakura, K. Uosaki and H. Kondoh, *Chem. Commun.*, 2013, **49**, 7848–7850.

75 M. Yoshida, T. Yomogida, T. Mineo, K. Nitta, K. Kato, T. Masuda, H. Nitani, H. Abe, S. Takakusagi, T. Uruga, K. Asakura, K. Uosaki and H. Kondoh, *J. Phys. Chem. C*, 2014, **118**, 24302–24309.

76 I. Zaharieva, D. González-Flores, B. Asfari, C. Pasquini, M. R. Mohammadi, K. Klingan, I. Zizak, S. Loos, P. Chernev and H. Dau, *Energy Environ. Sci.*, 2016, **9**, 2433–2443.

77 R. Frydendal, L. C. Seitz, D. Sokaras, T.-C. Weng, D. Nordlund, I. Chorkendorff, I. E. Stephens and T. F. Jaramillo, *Electrochim. Acta*, 2017, **230**, 22–28.

78 S. Tsunekawa, F. Yamamoto, K.-H. Wang, M. Nagasaka, H. Yuzawa, S. Takakusagi, H. Kondoh, K. Asakura, T. Kawai and M. Yoshida, *J. Phys. Chem. C*, 2020, **124**, 23611–23618.

79 M. F. Tesch, S. A. Bonke, R. Golnak, J. Xiao, A. N. Simonov and R. Schlögl, *Electrochem. Sci. Adv.*, 2022, **2**, e2100141.

80 E. A. Carbonio, J.-J. Velasco-Velez, R. Schlögl and A. Knop-Gericke, *J. Electrochem. Soc.*, 2020, **167**, 054509.

81 J.-J. Velasco-Vélez, L. J. Falling, D. Bernsmeier, M. J. Sear, P. C. J. Clark, T.-S. Chan, E. Stotz, M. Hävecker, R. Kraehnert, A. Knop-Gericke, C.-H. Chuang, D. E. Starr, M. Favaro and R. V. Mom, *J. Phys. D: Appl. Phys.*, 2021, **54**, 124003.

82 M. Risch, K. A. Stoerzinger, B. Han, T. Z. Regier, D. Peak, S. Y. Sayed, C. Wei, Z. Xu and Y. Shao-Horn, *J. Phys. Chem. C*, 2017, **121**, 17682–17692.

83 C. Schwanke, L. Xi and K. M. Lange, *J. Synchrotron Radiat.*, 2016, **23**, 1390–1394.

84 L. Xi, C. Schwanke, J. Xiao, F. F. Abdi, I. Zaharieva and K. M. Lange, *J. Phys. Chem. C*, 2017, **121**, 12003–12009.

85 L. Xi, F. Wang, C. Schwanke, F. F. Abdi, R. Golnak, S. Fiechter, K. Ellmer, R. van de Krol and K. M. Lange, *J. Phys. Chem. C*, 2017, **121**, 19668–19676.

86 M. Wiechen, H.-M. Berends and P. Kurz, *Dalton Trans.*, 2012, **41**, 21–31.

87 M. Salmanion, I. Kondov, M. Vandichel, P. Aleshkevych and M. M. Najafpour, *Inorg. Chem.*, 2022, **61**, 2292–2306.

This journal is © the Owner Societies 2023

Phys. Chem. Chem. Phys., 2023, **25**, 26958–26971 | **26971**